Magnonic frequency comb in the magnomechanical resonator

Guan-Ting Xu[1,2,3],[*] Mai Zhang[1,2,3],[*] Yu Wang[1,2], Zhen Shen[1,2,3],[†] Guang-Can Guo[1,2,3], and Chun-Hua Dong[1,2,3][‡]

[1]*CAS Key Laboratory of Quantum Information, University of Science and Technology of China,*
Hefei, Anhui 230026, People's Republic of China
[2]*CAS Center For Excellence in Quantum Information and Quantum Physics,*
University of Science and Technology of China, Hefei, Anhui 230088, People's Republic of China and
[3]*Hefei National Laboratory, University of Science and Technology of China,*
Hefei, Anhui 230088, People's Republic of China

An optical frequency comb is a spectrum of optical radiation which consists of evenly spaced and phase-coherent narrow spectral lines and is initially invented in laser for frequency metrology purposes. A direct analogue of frequency combs in the magnonic systems has not been demonstrated to date. In our experiment, we generate a new magnonic frequency comb in the resonator with giant mechanical oscillation through the magnomechanical interaction. We observe the magnonic frequency comb contains up to 20 comb lines, which are separated to the mechanical frequency of the 10.08 MHz. The thermal effect based on the strong pump power induces the cyclic oscillation of the magnon frequency shift, which leads to a periodic oscillation of the magnonic frequency comb. Moreover, we demonstrate the stabilization and control of the frequency spacing of the magnonic frequency comb via injection locking. Our work lays the groundwork of magnonic frequency combs for sensing and metrology.

A. Introduction

Optical frequency combs are composed of a set of equidistant coherent optical lines in the frequency domain. In the last two decades, they have exhibited rapid development in various fields [1–3], such as astronomy and cosmology, optical atomic clock [4], light detection and ranging (LiDAR) [5–7], low-noise microwave source [8–10], coherent optical communication [11, 12], quantum key distribution [13], dual-comb spectroscopy [14, 15], spectrometer [16, 17], and optical coherence tomography [18, 19]. Optical frequency combs in microresonators can be generated through electro-optical modulation or third-order Kerr nonlinearity $\chi^{(3)}$ [2]. Recently, mechanical vibration has been demonstrated for the generation and engineering of optical combs [20–24], which has attracted increasing attention due to its low repetition rate and suitability for acoustic sensing [25]. Furthermore, the frequency combs have also been well investigated beyond optical systems, such as microwave system and phononic system. However, the frequency comb in the magnonic system has not been demonstrated to date.

Magnons are the quantum of collective spin excitation of magnetization in ferromagnetic insulators such as yttrium iron garnet (YIG). They exhibit great frequency tunability, extremely low magnetic damping and high Curie temperature, making them an ideal carrier for performing coherent information processing, and precision measurements [26–31]. Similar to the traditional frequency comb, the magnonic frequency comb has been proposed for the development of high-precision magnonic frequency metrology and spectroscopy via the nonlinear interaction [32–34]. However, the weak nonlinear interaction of magnons presents a challenge for generating magnonic frequency combs [35]. Given the successful

of introduction mechanical vibration, the magnonic frequency comb based on magneto-mechanical coupling has been proposed in theory [36].

In this work, we experimentally generate a magnonic frequency comb in the resonator with giant mechanical oscillation through the magnomechanical interaction. This dynamical process is facilitated by an external pump that mimicked magnomechanical interactions mediated through the magnetostrictive effect. When the pump power is strong enough, magnomechanical nonlinearities play a significant role, and a self-induced nonlinear phenomenon similar to the Kerr-frequency comb effect can be observed in the magnomechanical system. We observe a magnonic frequency comb with up to 20 comb lines and a frequency spacing of 10.08 MHz, equaling the resonant frequency of the mechanical resonator. In this process, the strong pump field on the magnon is required, leading to a raised temperature of the magnon and a corresponding magnon frequency shift. Then, the magnonic frequency comb shows periodic oscillation due to the thermal effect. It is also in good agreement with the theoretical calculation based on the evolution equations of the magnon and phonon modes. Finally, we demonstrate the stabilization and control of the frequency spacing of the magnonic frequency comb via injection locking [37]. We can achieve tuning of comb teeth beyond a range of 1 kHz.

B. Experimental Results

Due to magnetostrictive forces, a type of radiation pressure-like interaction arises between the magnon mode and the mechanical mode, as shown in Fig. 1(a). When increasing the pump power to enhance the interaction, the self-induced nonlinear phenomena similar to
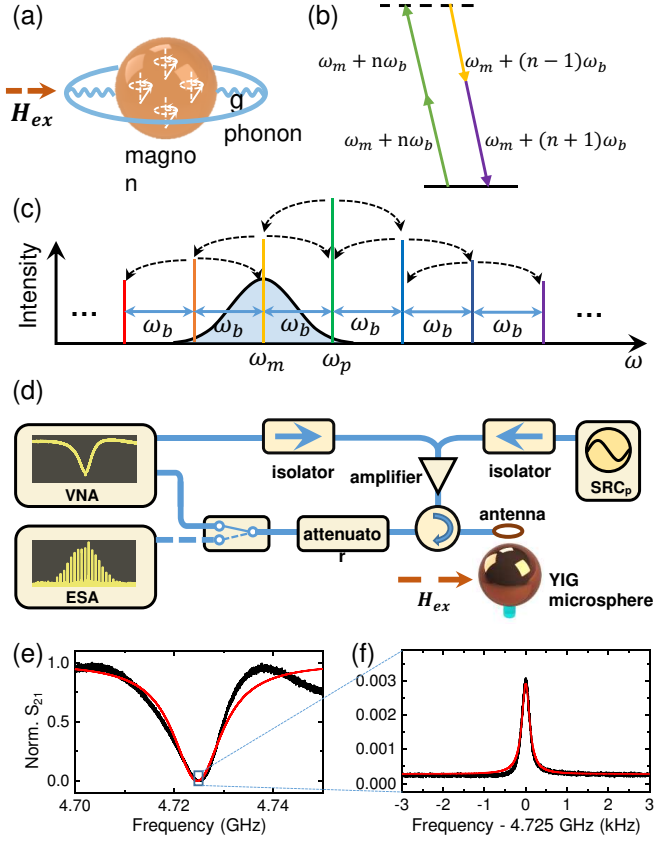
FIG. 1. (a) Illustration of the coupling between magnon and phonon with single magnon-phonon coupling strength g. (b) The magnonic frequency comb is generated via a two-magnon process. Two magnons with frequency $\omega_m + n\omega_b$ are annihilated to create two magnons with frequency $\omega_m + (n-1)\omega_b$ and $\omega_m + (n+1)\omega_b$, where the ω_m and ω_b are the frequency of the magnon and mechanical modes, respectively. (c) A cascaded two-magnon process is initiated to form a frequency comb separated with a mechanical frequency of ω_b. (d) Schematic of the experimental setup for the magnonic frequency comb. SRC: microwave source; VNA: vector network analyzer; ESA: electrical spectrum analyzer. (e) Measured microwave reflection spectrum around 4.725 GHz. (f) The detailed spectrum showing the mechanical mode in (e). The red lines are results of theoretical calculations discussed in the main text with the parameters of $g = 2.36$ mHz, $\kappa_m = 12$ MHz, $\kappa_b/2\pi = 220$ Hz and $\kappa_{in} = 6.1$ MHz.

the Kerr-frequency comb effect can be observed in the magnomechanical system based on the cascaded two-magnon process, as illustrated in Fig. 1(b-c). The two magnon process including two magnons with frequency of $\omega_m + n\omega_b$ are annihilated to create two magnons with frequency $\omega_m + (n-1)\omega_b$ and $\omega_m + (n+1)\omega_b$, where the ω_m and ω_b are the frequency of the magnon and mechanical modes, respectively. This initiates a cascaded process leading to the formation of a frequency comb with a free spectral range (FSR) of ω_b, the frequency relationship between the magnon frequency ω_m, mechanical frequency ω_b and pump frequency ω_p is given by $\omega_m = \omega_p - \omega_b$. The

interaction between the magnon and mechanical modes can be represented by the Hamiltonian expression:

$$
\begin{aligned}
H = & \left(\omega_m - \omega_p - i\tfrac{\kappa_m}{2}\right)m^\dagger m + \left(\omega_b - i\tfrac{\kappa_b}{2}\right)b^\dagger b \\
& + g\left(b^\dagger + b\right)m^\dagger m + i\sqrt{\kappa_{in}}\varepsilon_p\left(m^\dagger - m\right)
\end{aligned} \quad (1)
$$

where m and b are the annihilation operators of the magnon and mechanical modes, κ_m and κ_b represent the dissipation of magnon and phonon, respectively. g is the single magnon-phonon coupling strength, which depends on the overlap between magnon and phonon modes. ε_p is the pump field of the microwave with the frequency of ω_p. κ_{in} is the input coupling rate of the microwave. For the blue-detuned pump, the relationship between ω_m and ω_b satisfies $\Delta = \omega_p - \omega_m = \omega_b$.

As shown in the Hamiltonian, coupling between magnons and phonons leads to the phonon number dependent magnon frequency shift:

$$
\frac{dm}{dt} = \left\{i[-\Delta - g(b^\dagger + b)] - \frac{\kappa_m}{2}\right\}m + \sqrt{\kappa_{in}}\varepsilon_p, \quad (2)
$$

$$
\frac{db}{dt} = \left(i\omega_b - \frac{\kappa_b}{2}\right)b - igm^\dagger m. \quad (3)
$$

Like the frequency comb induced by the Kerr oscillator, when the pump condition exceeds the threshold of intra-cavity field instability, the mechanical mode starts to lasing. Modulated by the strongly lasing mechanical mode, magnon comb generates, where the amplitude of magnon mode will take a form as $m(t) = \sum_n m_n e^{i(\omega_m - \omega_p)t}e^{-in\omega_b t}, n \in Z$, where $m_n = \sqrt{\kappa_{in}}\varepsilon_p \sum_k \frac{J_{k-n}(\xi)J_n(-\xi)}{\kappa_m/2 - i(\Delta + k\omega_b)}$ and $\xi = 2gb/\omega_b$ is the normalized amplitude of mechanical mode. Meanwhile, the linewidth of mechanical mode is also narrowed significantly by the magnon comb that $\kappa_b' = \kappa_b - \chi$. As the narrow linewidth of the mechanical mode, the no-coherence part of the magnon pump can be ignored and there is $\chi = 2g\sum_n \text{Im}[m_n^\dagger m_{n+1}]/b$. When $\kappa_b' \leq 0$, the system is unstable and a magnon comb occurs.

The experiment setup is illustrated in Fig. 1(d). Initially, a YIG microsphere with a diameter of 623.6 μm is subject to a bias magnetic field H_{ex} aligned parallel to the equatorial plane of the YIG microsphere, which supports a uniform magnon mode. The relation between the frequency of the magnon and magnetic field intensity follows the equation $\omega_m = \gamma H_{ex}$, where $\gamma = 2\pi \times 2.8$ MHz/Oe represents the gyromagnetic ratio. In order to excite the magnon mode, we employ an antenna located close to the YIG microsphere with a frequency around 4.725 GHz. Fig. 1(e) shows the magnon resonance through the microwave reflection spectrum S_{21} obtained by a vector network analyzer (VNA), corresponding to a dissipation rate of $\kappa_m = 12$ MHz. The frequency associated with the mechanical mode is obtained $\omega_b/2\pi = 10.08$ MHz [31, 38]. The dissipation rate of the mechanical mode is $\kappa_b/2\pi = 220$ Hz, as shown in Fig.1(f). Meanwhile
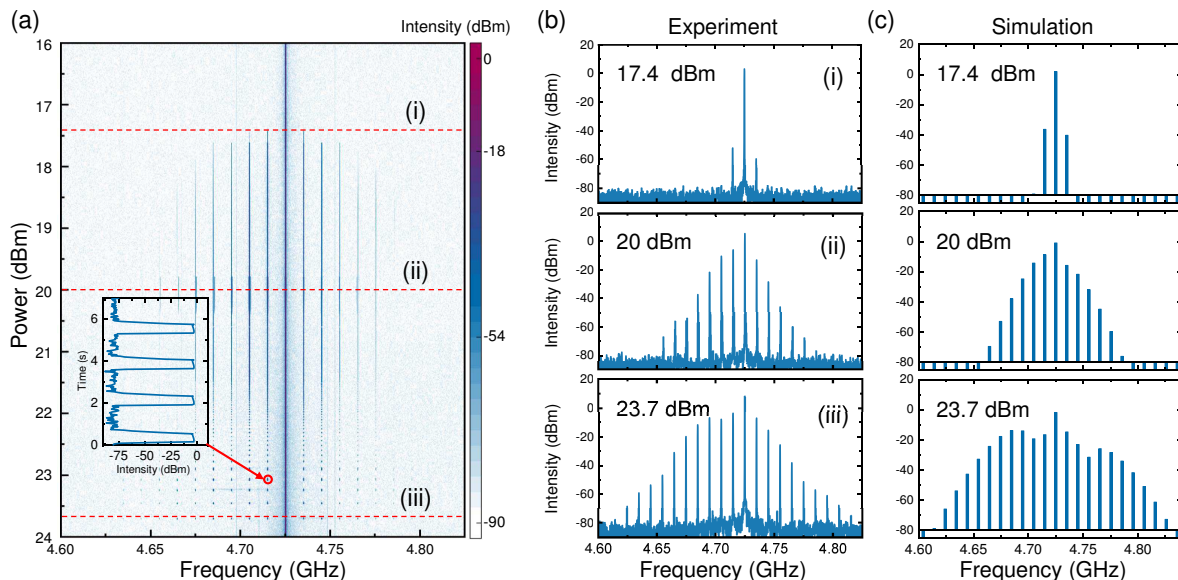
FIG. 2. (a) Evolution of the magnonic frequency comb along increased pump power from 16 dBm to 24 dBm with the frequency of $\omega_p = 4.725$ GHz. The inset shows the evolution of the spectrum over a period of 7 seconds at a power of 23.1 dBm and frequency $\omega_p - \omega_b = 4.714$ GHz component. (b) Snapshots with different evolution stages in (a). (c) The simulated spectra of the magnonic frequency combs with the same conditions in (b).

the pump field of the microwave with the frequency of $\omega_p = 4.725$ GHz. Based on these interactions, the theoretical calculations are achieved with the parameter of the single magnon-phonon coupling strength $g = 2.36$ mHz and the input coupling rate of microwave $\kappa_{in} = 6.1$ MHz.

Figure 2 displays the spectra of the magnonic frequency comb with varying pump power from 16 dBm to 24 dBm at the frequency of $\omega_p = 4.725$ GHz. For a weak microwave pump field, i. e., below the threshold of 17.4 dBm, the spectrum only contains the pump component, with no comb lines. As the pump power gradually increases to reach the threshold for generating comb conditions, a frequency comb emerges, as shown in Fig. 2(b), with a tooth spacing of $\omega_b = 10.08$ MHz. The number of comb lines increases steadily with higher pump power. The typical magnonic frequency comb can have up to 21 comb lines with the pump power at 23.7dBm. Figure 2(c) displays magnonic frequency combs obtained from numerical simulations under the pump power of 17.4 dBm, 20 dBm, and 23.6 dBm, respectively. Since strong pump heats the system, magnon mode is red shifted due to the thermal effect and the effective detuning between pump frequency and magnon frequency $\Delta\omega_{eff}$ are $1.1\omega_b$, $1.3\omega_b$ and $2\omega_b$, respectively at those pump powers above. These inconsistent detunings are mainly caused by thermal effects, which we will discuss later. Other numerical simulation parameters are consistent with the experiment.

During the process of increasing pump power, it is observed that when the pump power reached 21.4 dBm, the comb teeth become unstable and oscillate in the time domain, with the oscillation period increasing as the power

increases. The inset of Fig. 2(a) shows the evolution of a typical comb line over a period of 7 seconds at a power of 23.1 dBm at a frequency of $\omega_p - \omega_b = 4.714$ GHz. To investigate the physical mechanism for this oscillation, we further investigate the dynamic evolution of the magnon mode. When we fix the pump frequency at $\omega_p = 4.725$ GHz and the power at 23.1 dBm, we observe the temporal evolution of the S_{21} spectrum measured by a vector network analyzer (VNA), as shown in Fig. 3(a). The comb generation exhibits a periodicity of $T = 1.7$ s, corresponding to the period shown in the inset of Fig. 2(a). Figure 3(b-c) show the typical S_{21} spectrum at $t = 2$ s and 3 s in Fig. 3(a), respectively. When the pump power is very strong, an artifact signal peak will appear at the overlap of the comb tooth frequency (4.714 GHz) in the S_{21} spectrum, and its frequency is related to the resolution bandwidth of the VNA. In addition, the oscillation time scale is similar to that of thermal relaxation [24, 39]. We conduct further analysis to investigate the thermal effect during tooth generation. With a large amount of energy coupled into the system, the YIG sphere will be heated:

$$\frac{d\delta T}{dt} = -\frac{1}{\tau}\delta T + \frac{\kappa_{in}\hbar\omega_p m^\dagger m}{c_p}, \quad (4)$$

where δT is the temperature difference between YIG and environment, $\tau = 1.6$ s is the thermal relaxation time, $c_p = 9.55 \times 10^{-3}$ J/K is the thermal capacity of the YIG sphere and $\kappa_{in} = \kappa_m - \kappa_{ex}$ is the intrinsic dissipation rate. As a result, the frequency of the magnon mode will

be red shifted with the increasing temperature:

$$\omega'_m = \omega_m - \alpha_{\text{T}}(\delta T - \delta T_0), \qquad (5)$$

where $\alpha_{\text{T}} = 0.41$ MHz/K is the frequency shift per unit temperature change and $\delta T_0 = 4.2$ K is the initially temperature difference. Figure 3(d) depicts the threshold curve of phonon amplitude versus detuning, where $\kappa'_b = 0$. Points on the curve indicate steady states. For states under the curve corresponding to the shaded fill area in Fig. 3(d), there is $\kappa'_b < 0$ and phonon amplitude will increase. Conversely, for states above the curve corresponding to the blank space in Fig. 3(d), there is $\kappa'_b > 0$ and the phonon amplitude will decrease. Moreover, as shown in Fig. 3(d), this process can be divided into four processes: (1) When the threshold is approached, a large number of magnons are generated, causing the YIG sphere to heat up and leading to a red shift in the magnon frequency due to thermal effects. (2) When the frequency shift is substantial enough, the threshold cannot be approached for all amplitudes of the mechanical mode. At this time, the magnon number will dramatically decrease due to the large detuning between resonances. (3) The YIG sphere will no longer heat up, and the heat will be dissipated into the ambient air, causing the magnon frequency to shift back in the direction of high frequency. (4) If the pump power remains constant, the magnon frequency will return to the point where the threshold can be reached, and comb teeth are generated. Then the state of the system comes back to process (1) and the oscillation will repeat steadily. We examine the frequency shift and oscillation period change under different pump powers, as shown in Fig. 3(e-f). We find that the frequency shift varied from 1 MHz to 7 MHz, while the oscillation period increased from 0.4 s to 1.7 s with increasing pump power. This phenomenon is due to the different heating rates of the YIG sphere with varying pump power, which agrees well with the numerical calculations.

As the stabilization and control of the magnonic frequency comb are critical for the potential application of high-precision magnonic frequency spectroscopy, here, we also demonstrate the stabilization and control of the frequency spacing of the magnonic frequency comb via injection locking [37], which significantly suppresses the instability of the comb teeth, as shown in Fig. 4(a). An additional source is injected into the YIG microsphere at a frequency of 4.71492 GHz. Prior to turning on the external source, the magnonic frequency comb is generated, and the comb tooth on the RF spectrum is unstable (stage I), particularly when focusing on the comb line at 4.71492 GHz. We then turn on the external source, and the stabilization of the magnonic frequency comb is notably improved (stage II). Finally, by turning off the external source, the stable comb tooth immediately returns to the initial state and becomes as unstable as before (stage III). Furthermore, we study the locking range
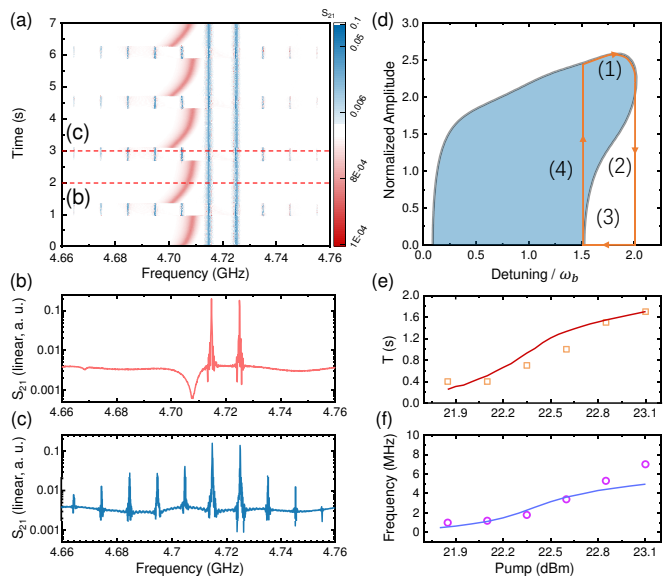

FIG. 3. (a) Evolution of the S_{21} spectrum along time (within 7 seconds) with the pump power of 23.1 dBm and frequency of $\omega_p = 4.725$ GHz. (b-c) The typical S_{21} spectrum under $t = 2$ s and 3 s in (a). (d) Threshold curve for phonon amplitude and detuning at the pump power of 23.1 dBm. (e-f) The oscillation period and the frequency shift versus pump power from 21.85 dBm to 23.1 dBm. The solid line is the theoretical curve.

of this injection locking scheme. Figure 4(b) displays the evolution of the RF spectra with a power of -6.4 dBm when the external source frequency slowly varied. Initially, when the frequency difference between the external source and comb line is relatively large, beat notes of the initial frequency and external source frequency and their harmonic components all existe in the RF spectrum. As we continue scanning, the comb is injection locked by the external source when their frequency difference is very close. Scanning in the same direction further led to the external source frequency crossing the comb line and going out of the locking range at last. The locking range increases with the enhancement of the external source power, up to a maximum of 1.2 kHz, as depicted in Fig. 4(c).

C. Discussion

In conclusion, we demonstrate a magnonic frequency comb in the magnomechanical resonator. The magnonic frequency comb has up to 20 comb lines and a frequency spacing 10.08 MHz, equaling the resonant frequency of the mechanical mode. Additionally, we study the thermal effect involved in the frequency comb generation process, where the frequency comb exhibits periodic oscillation dependent on pump power. Our experimental results are in agreement with numerical calculations. Furthermore,
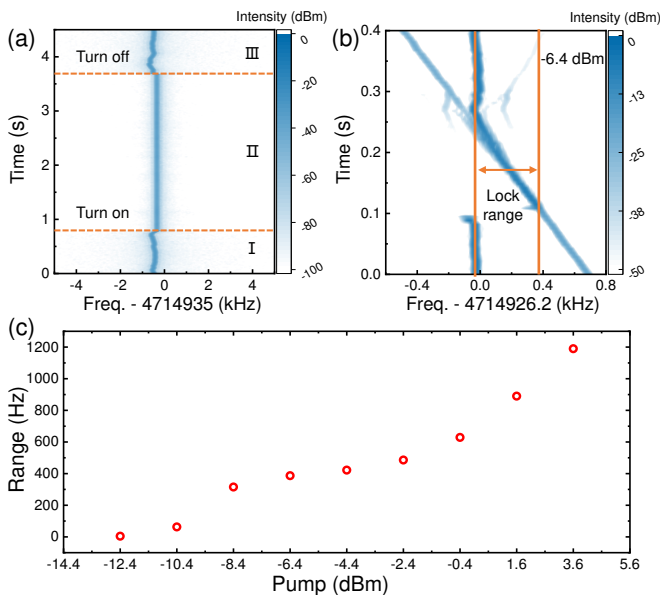
FIG. 4. (a) Evolution of one comb tooth when the external source is on and off. The initial comb tooth is unstable (I). The comb tooth is synchronized to the external source (II). The comb tooth returns to the initial state after turning off the external source (III). (b) Evolution of the RF spectrum with varied injected frequency. The injected power is -6.4 dBm, and the comb is synchronized to the external source when the frequency difference is less than 400 Hz. (c) Locking ranges with varied pump power.

we demonstrate the stabilization and control of the frequency spacing of the magnonic frequency comb via injection locking. We can achieve tuning of comb teeth beyond a range of 1 kHz. Our work not only advances the study of nonlinear physics in magnonic system but also unlocks the potential of magnonic frequency combs for sensing and metrology.

* These authors contributed equally to this work.
† shenzhen@ustc.edu.cn
‡ chunhua@ustc.edu.cn

[1] T. J. Kippenberg, R. Holzwarth, and S. A. Diddams, "Microresonator-based optical frequency combs," Science **332**, 555 (2011).

[2] T. J. Kippenberg, A. L. Gaeta, M. Lipson, and M. L. Gorodetsky, "Dissipative kerr solitons in optical microresonators," Science **361**, eaan8083 (2018).

[3] S. A. Diddams, K. Vahala, and T. Udem, "Optical frequency combs: Coherently uniting the electromagnetic spectrum," Science **369**, eaay3676 (2020).

[4] Z. L. Newman, V. Maurice, T. Drake, J. R. Stone, T. C. Briles, D. T. Spencer, C. Fredrick, Q. Li, D. Westly, B. R. Ilic, *et al.*, "Architecture for the photonic integration of an optical atomic clock," Optica **6**, 680 (2019).

[5] M.-G. Suh and K. J. Vahala, "Soliton microcomb range measurement," Science **359**, 884 (2018).

[6] P. Trocha, M. Karpov, D. Ganin, M. H. Pfeiffer, A. Kordts, S. Wolf, J. Krockenberger, P. Marin-Palomo, C. Weimann, S. Randel, *et al.*, "Ultrafast optical ranging using microresonator soliton frequency combs," Science **359**, 887 (2018).

[7] J. Wang, Z. Lu, W. Wang, F. Zhang, J. Chen, Y. Wang, J. Zheng, S. T. Chu, W. Zhao, B. E. Little, *et al.*, "Long-distance ranging with high precision using a soliton microcomb," Photonics Research **8**, 1964 (2020).

[8] W. Liang, D. Eliyahu, V. S. Ilchenko, A. A. Savchenkov, A. B. Matsko, D. Seidel, and L. Maleki, "High spectral purity kerr frequency comb radio frequency photonic oscillator," Nature Communications **6**, 7957 (2015).

[9] E. Lucas, P. Brochard, R. Bouchand, S. Schilt, T. Südmeyer, and T. J. Kippenberg, "Ultralow-noise photonic microwave synthesis using a soliton microcomb-based transfer oscillator," Nature Communications **11**, 374 (2020).

[10] J. Liu, E. Lucas, A. S. Raja, J. He, J. Riemensberger, R. N. Wang, M. Karpov, H. Guo, R. Bouchand, and T. J. Kippenberg, "Photonic microwave generation in the x- and k-band using integrated soliton microcombs," Nature Photonics **14**, 486 (2020).

[11] P. Marin-Palomo, J. N. Kemal, M. Karpov, A. Kordts, J. Pfeifle, M. H. Pfeiffer, P. Trocha, S. Wolf, V. Brasch, M. H. Anderson, *et al.*, "Microresonator-based solitons for massively parallel coherent optical communications," Nature **546**, 274 (2017).

[12] B. Corcoran, M. Tan, X. Xu, A. Boes, J. Wu, T. G. Nguyen, S. T. Chu, B. E. Little, R. Morandotti, A. Mitchell, *et al.*, "Ultra-dense optical data transmission over standard fibre with a single chip source," Nature Communications **11**, 2568 (2020).

[13] F.-X. Wang, W. Wang, R. Niu, X. Wang, C.-L. Zou, C.-H. Dong, B. E. Little, S. T. Chu, H. Liu, P. Hao, *et al.*, "Quantum key distribution with on-chip dissipative kerr soliton," Laser & Photonics Reviews **14**, 1900190 (2020).

[14] M.-G. Suh, Q.-F. Yang, K. Y. Yang, X. Yi, and K. J. Vahala, "Microresonator soliton dual-comb spectroscopy," Science **354**, 600 (2016).

[15] M. Yu, Y. Okawachi, A. G. Griffith, N. Picqué, M. Lipson, and A. L. Gaeta, "Silicon-chip-based mid-infrared dual-comb spectroscopy," Nature Communications **9**,

1869 (2018).

[16] Q.-F. Yang, B. Shen, H. Wang, M. Tran, Z. Zhang, K. Y. Yang, L. Wu, C. Bao, J. Bowers, A. Yariv, *et al.*, "Vernier spectrometer using counterpropagating soliton microcombs," Science **363**, 965 (2019).

[17] R. Niu, M. Li, S. Wan, Y. R. Sun, S.-M. Hu, C.-L. Zou, G.-C. Guo, and C.-H. Dong, "khz-precision wavemeter based on reconfigurable microsoliton," Nature Communications **14**, 169 (2023).

[18] X. Ji, X. Yao, A. Klenner, Y. Gan, A. L. Gaeta, C. P. Hendon, and M. Lipson, "Chip-based frequency comb sources for optical coherence tomography," Optics Express **27**, 19896 (2019).

[19] P. J. Marchand, J. Riemensberger, J. C. Skehan, J.-J. Ho, M. H. Pfeiffer, J. Liu, C. Hauger, T. Lasser, and T. J. Kippenberg, "Soliton microcomb based spectral domain optical coherence tomography," Nature Communications **12**, 427 (2021).

[20] L. Cao, D. Qi, R. Peng, M. Wang, and P. Schmelcher, "Phononic frequency combs through nonlinear resonances," Physical Review Letters **112**, 075505 (2014).

[21] M. H. de Jong, A. Ganesan, A. Cupertino, S. Gröblacher, and R. A. Norte, "Mechanical overtone frequency combs," Nature Communications **14**, 1458 (2023).

[22] A. Ganesan, C. Do, and A. Seshia, "Phononic frequency comb via intrinsic three-wave mixing," Physical Review Letters **118**, 033903 (2017).

[23] M.-A. Miri, G. D'Aguanno, and A. Alù, "Optomechanical frequency combs," New Journal of Physics **20**, 043013 (2018).

[24] Y. Hu, S. Ding, Y. Qin, J. Gu, W. Wan, M. Xiao, and X. Jiang, "Generation of optical frequency comb via giant optomechanical oscillation," Physical Review Letters **127**, 134301 (2021).

[25] J. Zhang, B. Peng, S. Kim, F. Monifi, X. Jiang, Y. Li, P. Yu, L. Liu, Y.-x. Liu, A. Alù, *et al.*, "Optomechanical dissipative solitons," Nature **600**, 75 (2021).

[26] A. Serga, A. Chumak, and B. Hillebrands, "Yig magnonics," Journal of Physics D: Applied Physics **43**, 264002 (2010).

[27] B. Lenk, H. Ulrichs, F. Garbs, and M. Münzenberg, "The building blocks of magnonics," Physics Reports **507**, 107 (2011).

[28] Z.-X. Liu, C. You, B. Wang, H. Xiong, and Y. Wu, "Phase-mediated magnon chaos-order transition in cavity optomagnonics," Optics Letters **44**, 507 (2019).

[29] H. Wang, J. Chen, T. Liu, J. Zhang, K. Baumgaertl, C. Guo, Y. Li, C. Liu, P. Che, S. Tu, *et al.*, "Chiral spin-wave velocities induced by all-garnet interfacial dzyaloshinskii-moriya interaction in ultrathin yttrium iron garnet films," Physical Review Letters **124**, 027203 (2020).

[30] C.-Z. Chai, Z. Shen, Y.-L. Zhang, H.-Q. Zhao, G.-C. Guo, C.-L. Zou, and C.-H. Dong, "Single-sideband microwave-to-optical conversion in high-q ferrimagnetic microspheres," Photonics Research **10**, 820 (2022).

[31] Z. Shen, G.-T. Xu, M. Zhang, Y.-L. Zhang, Y. Wang, C.-Z. Chai, C.-L. Zou, G.-C. Guo, and C.-H. Dong, "Coherent coupling between phonons, magnons, and photons," Physical Review Letters **129**, 243601 (2022).

[32] J. Rao, B. Yao, C. Wang, C. Zhang, T. Yu, and W. Lu, "Unveiling a pump-induced magnon mode via its strong interaction with walker modes," Physical Review Letters **130**, 046705 (2023).

[33] Z. Wang, H. Yuan, Y. Cao, Z.-X. Li, R. A. Duine, and P. Yan, "Magnonic frequency comb through nonlinear magnon-skyrmion scattering," Physical Review Letters **127**, 037202 (2021).

[34] Z. Wang, H. Yuan, Y. Cao, and P. Yan, "Twisted magnon frequency comb and penrose superradiance," Physical Review Letters **129**, 107203 (2022).

[35] Z.-X. Liu and Y.-Q. Li, "Optomagnonic frequency combs," Photonics Research **10**, 2786 (2022).

[36] H. Xiong, "Magnonic frequency combs based on the resonantly enhanced magnetostrictive effect," Fundamental Research **3**, 8 (2023).

[37] S. Wan, R. Niu, Z.-Y. Wang, J.-L. Peng, M. Li, J. Li, G.-C. Guo, C.-L. Zou, and C.-H. Dong, "Frequency stabilization and tuning of breathing solitons in Si_3N_4 microresonators," Photonics Research **8**, 1342 (2020).

[38] G.-T. Xu, M. Zhang, Z.-Y. Wang, Y. Wang, Y.-X. Liu, Z. Shen, G.-C. Guo, and C.-H. Dong, "Ringing spectroscopy in the magnomechanical system," Fundamental Research **3**, 45 (2023).

[39] T. Carmon, L. Yang, and K. J. Vahala, "Dynamical thermal behavior and thermal self-stability of microcavities," Optics Express **12**, 4742 (2004).